Superlattices and Microstructures, Vol. 20, No. 4, 1996

Zeeman splitting of single semiconductor impurities in resonant tunneling heterostructures

M. R. Deshpande, J. W. Sleight†, M. A. Reed, R. G. Wheeler
Departments of Physics, Applied Physics, and Electrical Engineering, Yale University, P.O. Box 208120, New Haven, CT 06520, U.S.A.

R. J. Matyi‡
Central Research Laboratories, Texas Instruments Incorporated, Dallas, TX 75265, U.S.A.

(Received 20 May 1996)

Zeeman splitting of the ground state of single impurities in the quantum wells of resonant tunneling heterostructures is reported. We determine the absolute magnitude of the effective magnetic spin splitting factor $g^*_\perp$ for a single impurity in a 44 Å $Al_{0.27}Ga_{0.73}As/GaAs/Al_{0.27}Ga_{0.73}As$ quantum well to be 0.28 ± 0.02. This system also allows for independent measurement of the electron tunneling rates through the two potential barriers and estimation of the occupation probability of the impurity state in the quantum well.

© 1996 Academic Press Limited

Key words: resonant tunneling heterostructures, spin g factor, electron tunneling rates.

1. Introduction

The experimental realization of granular electronic systems, such as low dimensional semiconductor and ultra small metallic systems, has focused attention on the basic physical properties of discrete systems. Especially intriguing are the semiconductor quantum dot [1–5] and the physically similar localized impurity state tunneling systems [6–11]. The latter provides a unique laboratory for the study of a single impurity. We present here the first observation of Zeeman spin splitting of a single semiconductor impurity, studied by tunneling transport. The measured g^* factor provides an important test of the band theory of confined semiconductor systems, and our method is particularly important for well widths less than 50 Å where other methods are less precise [12–14].

Isolated donor impurities in the quantum well regions of large area resonant tunneling heterostructures form localized ($\sim$ 100 Å) hydrogenic states bound to the quantum eigenstates. Figure 1 illustrates a band diagram of the structure used in this study with one impurity state in the well schematically noted. Under applied bias, as the impurity state aligns with the emitter Fermi level, the current exhibits a step-like increase (Fig. 2). In general, there may be multiple impurities giving rise to multiple, overlapping steps in the current–voltage ($I(V)$)

† Present address: Digital Semiconductor, Hudson, MA, U.S.A.

‡ Present address: Department of Materials Science and Engineering, University of Wisconsin at Madison, WI, U.S.A.

0749–6036/96/080513 + 10 \$25.00/0

© 1996 Academic Press Limited

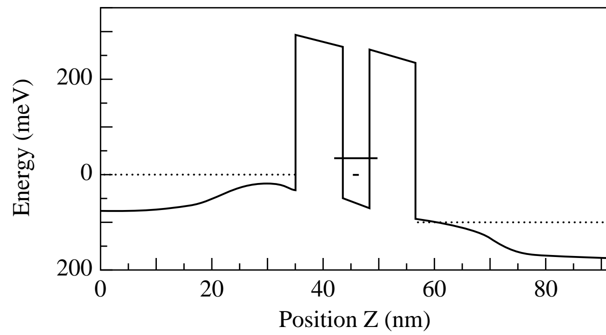

Fig. 1. Model conduction band diagram of the device, at an applied bias of 100 mV, showing the quantum eigenstate (long line) and a localized impurity state (short line) in the well. The dotted line represents the Fermi level in the leads.

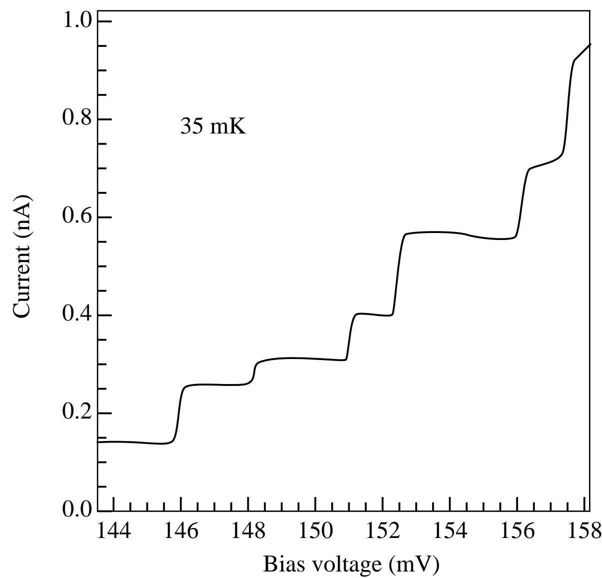

Fig. 2. $I(V)$ characteristics (zero magnetic field, $T_{mix} = 35$ mK) of the quantum well device ($w = 8.5$ nm) showing the pre-threshold region with sharp step-like structures. The various current steps are attributed to tunneling through separate impurity states in the well.

characteristics. An appropriately dilute, unintentional doping concentration gives rise to isolated, uncorrelated impurities, allowing measurement of a single one. In a magnetic field the spin degeneracy of the impurity ground state is broken, which results in a splitting of the current step in the $I(V)$ characteristics. The magnitude of the spin g^* factor can be determined from the voltage difference between the two fragments of the spin–split step. The current magnitudes of the two fragments enable us, for the first time, to independently determine the electron tunneling rates through the two potential barriers in a sequential tunneling picture [4, 15].

2. Sample design

The nominally symmetric resonant tunneling heterostructures are grown by molecular beam epitaxy (MBE) on a Si-doped GaAs (100) substrate [16]. The epitaxial layers consist of a 1.8×10^{18} cm^{-3} Si-doped GaAs

contact, a 15 nm undoped GaAs spacer layer, an undoped $Al_{0.27}Ga_{0.73}As$ bottom barrier of width w, a 4.4 nm undoped GaAs quantum well, an undoped $Al_{0.27}Ga_{0.73}As$ top barrier of the same width w, a 15 nm undoped GaAs spacer layer, and a 1.8×10^{18} cm^{-3} Si doped GaAs top contact. We study devices with two different barrier widths ($w = 8.5$ nm and 6.5 nm). Square mesas with lateral dimensions from 2 μm to 64 μm are fabricated using standard photolithography techniques. Two terminal $I(V)$ characteristics are measured in a dilution refrigerator with a mixing chamber temperature (T_{mix}) of 35 mK.

3. Observations

3.1. Tunneling through impurities

Figure 2 shows the $I(V)$ characteristics for a typical device (64 μm^2, $T_{mix} = 35$ mK, $w = 8.5$ nm) showing the sharp steps in the $I(V)$ characteristics. This step structure is observed to be sample specific, but for a given sample it is exactly reproducible. Similar steps are observed in other devices with different barrier thicknesses. The step current magnitudes are observed to be of the order of e/τ (e is the electronic charge and τ is the lifetime of the quantum well state as estimated from a bandprofile model [9]). This suggests that the current steps are due to single electron tunneling through individual, zero dimensional states in the quantum well. Similar features have been observed and reported previously [6, 7], and the various current steps are attributed to tunneling through bound states of separate impurities in the quantum well.

3.2. Spin splitting

Figure 3 shows an expanded view of the first current step edge at 35 mK for forward and reverse bias at 0 T and at 9 T. The magnetic field is oriented perpendicular to the current direction (parallel to the heterointerfaces). At zero field, the ground state of the impurity is spin degenerate leading to a single current step. Upon lifting of the degeneracy at finite field, a splitting of the current step is observed†. Figure 4 shows the dependence of the $I(V)$ characteristics upon increasing magnetic field. Note that the spin splitting increases as the field is swept from 0 T (bottom) to 9 T (top). Figure 5 shows the voltage separation between the corresponding two spin-split conductance peaks which increases linearly with the magnetic field strength as expected. Due to the finite widths of the conductance peaks, it is not possible to resolve the splitting for magnetic fields less than 5.5 T. The best line fit to the data (Fig. 5) closely intersects $\Delta V = 0$ at $B = 0$ and has a slope $g_\perp^* \mu_B/\alpha$, where μ_B is the Bohr magneton, $g_\perp^*$ is the effective gyromagnetic ratio of the impurity with the magnetic field perpendicular to the growth direction of the quantum well and α is the voltage to energy conversion factor [4, 5, 8, 11].

3.2.1. Determination of α

To determine the spin g^* factor it is necessary to know the voltage to energy conversion factor, α, which is accurately determined by studying the thermal broadening of the current step. The current through a localized impurity state in the quantum well, at bias V and temperature T, depends upon the density of occupied electronic states in the emitter at the same energy as the impurity state, which is proportional to the Fermi distribution function f. As shown in Fig. 6, the current plateau edges exhibit characteristic Fermi level thermal broadening. We can express the current as

$$I(V, T) = 2I_{th} f(V, T) = \frac{2I_{th}}{1 + \exp[\alpha e(V_{th} - V)/kT]} \quad (1)$$

† Splitting is also observed when the magnetic field is parallel to the current direction. We restrict this paper to the case of magnetic field perpendicular to current.

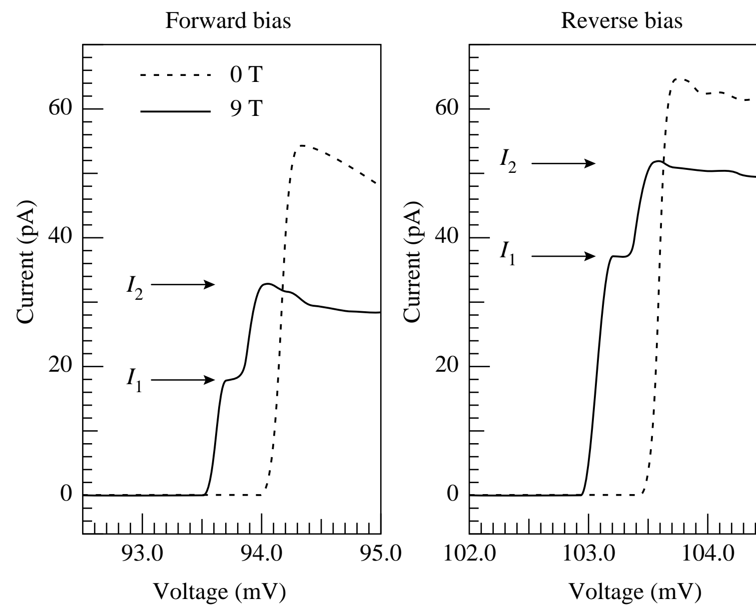

Fig. 3. $I(V)$ characteristics at $T_{mix} = 35$ mK of the first current step edge in forward bias (left) and reverse bias (right) at 0 T (– – –) and 9 T (——). I_1 and I_2 mark the current values at 9 T as shown. I_1 gives the current of the first fragment while I_2 is the net current of both fragments of the split step edge.

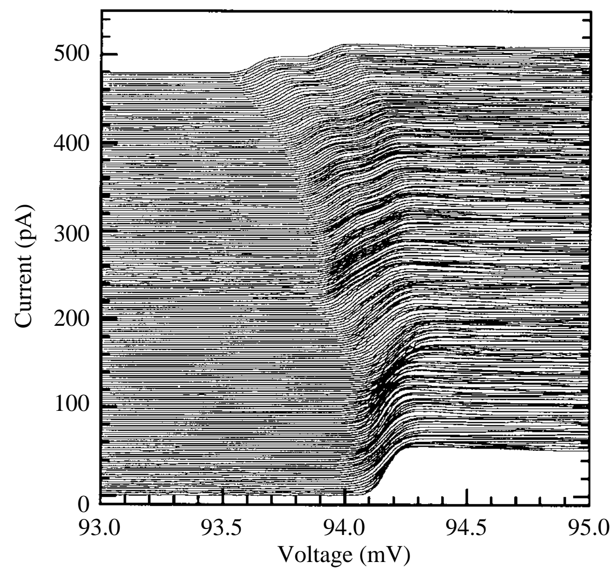

Fig. 4. $I(V)$ characteristics ($T_{mix} = 35$ mK) of the first current step edge in forward bias of the 8.5 nm barrier device in increasing magnetic fields from 0 T (bottom) to 9 T (top). The curves are vertically offset for clarity.

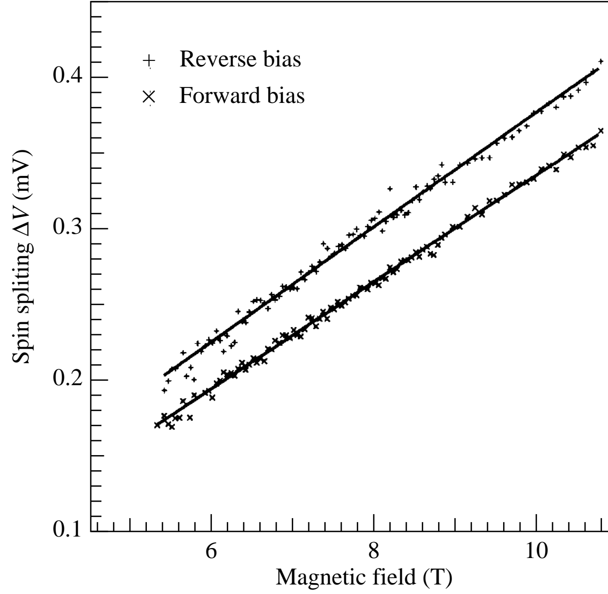

Fig. 5. The experimental spin splitting versus magnetic field perpendicular to current for the first current step of the 8.5 nm barrier device in forward and reverse bias at $T_{mix} = 35$ mK. The solid lines are linear fits to the data.

where e is the electron charge, k is Boltzmann's constant, and V_{th} and I_{th} are the threshold voltage and current at the observed common intersection point of the various $I(V)$ curves at different temperatures. The only free parameter α, is determined from a fit (Fig. 6) of the above Fermi function to the $I(V)$ traces at zero magnetic field. The fits are done for data taken at different temperatures, from 0.5 to 5 K, and α is determined for each. The average value of α along with the rms error is reported. For the device with 8.5 nm barrier $\alpha = 0.48 \pm 0.02$ for forward bias and 0.42 ± 0.02 for reverse bias. For the device with 6.5 nm barrier $\alpha = 0.40 \pm 0.02$ for forward bias. The fits are done for the region $V \leq V_{th}$ when the current is small and not affected by the occupancy of the impurity state.

3.2.2. Determination of g^* factor

From these values of α and the measured spin splitting in voltage, the absolute magnitude of the spin $g^*_\perp$ value of the impurities is determined. For the device with 8.5 nm barrier we determine the g^* factor for two separate impurity steps in both forward and reverse bias directions. We obtain for the first impurity, $g^*_\perp = (0.28 \pm 0.02, 0.28 \pm 0.02)$ (for forward and reverse bias, respectively) and for the second impurity, $g^*_\perp = (0.28 \pm 0.02, 0.27 \pm 0.02)$. For the device with 6.5 nm barrier we study only one impurity in forward bias for which we get $g^*_\perp = (0.27 \pm 0.02)$.

The g^* value of electrons in bulk GaAs (-0.44) is different from the free electron value ($+2$) because of the spin orbit interaction in the valence band and its effect on the conduction band as analyzed using $\vec{k} \cdot \vec{p}$ theory. In confined quantum well regions, it changes further and also becomes anisotropic. This is partly caused by the change in the electron and hole energies due to confinement, and partly due to the electron wavefunction penetration in the barrier material where the electron has a higher g^* value ($+0.39$). g^* is theoretically predicted to be a strong function of the quantum well width and changes from the bulk value

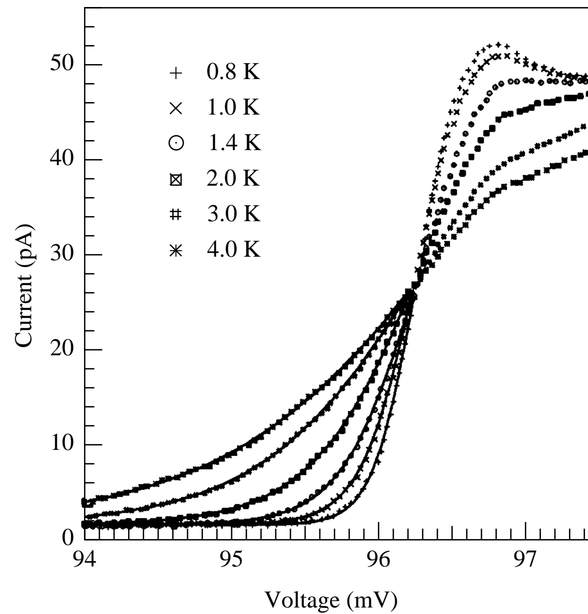

Fig. 6. $I(V)$ characteristics of the first impurity current step edge of the 8.5 nm barrier device at different temperatures showing the Fermi level broadening and the Fermi fit to these $I(V)$ traces.

of -0.44 to greater than $+0.4$ for well widths less than 30 Å [12]. Our measurement is consistent with this prediction and with recent experimental results [13, 14] (assuming here that the sign of g^* is positive).

Due to the 3D nature of the emitter, at any given energy electrons of both spin orientations are available for tunneling (even with applied magnetic field). Figure 7 shows thermal broadening of the first current step edge split at 9 T. Separate Fermi broadening of the two fragments of the split step indicates that in both cases electrons involved in tunneling are the Fermi electrons in the emitter. The observed experimental voltage difference is thus entirely due to the spin splitting of the impurity state, and is not affected by the g^*-factor of the electrons in the emitter †. We also note that electron–electron interactions will not alter the relative energy of the two spin states and thus the measured g^* factor. Coulomb interaction between the tunneling electron and the electrons in the emitter causes a rise in the step current near the threshold at low temperatures, which is observed (as first reported by Geim *et al.* [8]), but it should not affect the energy separation of the two spin states.

3.3. Determination of tunneling rates

Analysis of the tunneling current through the spin–split system yields additional information about the tunneling process. Recalling Fig. 3, the two fragments of the spin–split step at 9 T are observed *not* to have the same current magnitude ($(I_2 - I_1) \neq I_1$). This difference is more prominent in reverse bias. To analyze this, we define Γ_b and Γ_t to be the tunneling rates for an electron to tunnel through the bottom and the top (referred to growth direction) potential barriers, respectively, of the double barrier heterostructure. We also define Γ_{cl} and Γ_{em} to be the electron tunneling rates through the collector (downstream) and emitter (upstream) (referred to electron flow direction) potential barriers. In forward bias, electron injection is through the top barrier into

† If the Fermi energy in the emitter is small and weakly localized states are formed in the emitter, the g^*-factor of these weakly localized states would have to be taken into account as reported by Sakai *et al.* [10].

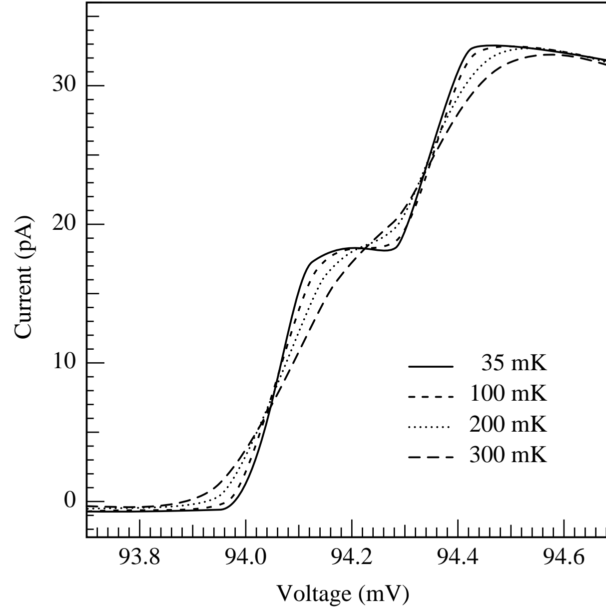

Fig. 7. $I(V)$ characteristics at 9 T showing the spin–split first current step edge in forward bias at mixing chamber temperatures ranging from 35 to 300 mK.

the quantum well ($\Gamma_{em} \equiv \Gamma_t$, $\Gamma_{cl} \equiv \Gamma_b$), while in reverse bias, electron injection is through the bottom barrier into the quantum well ($\Gamma_{em} \equiv \Gamma_b$, $\Gamma_{cl} \equiv \Gamma_t$). We also define p to be the occupation probability for an electron in a localized state in the quantum well. In the sequential tunneling picture, $p = f\Gamma_{em}/(\Gamma_{em} + \Gamma_{cl})$. Since the spin splitting energy ($\Delta E \leq 150$ μeV) is much smaller than the barrier potential energy (≈ 300 meV), we assume that the tunneling rates are the same for electrons tunneling through the spin up or the spin down states irrespective of the slight energy difference. We also assume that the emitter electrons are not spin polarized which is a good assumption since the Fermi energy (~ 40 meV) is much larger than the spin splitting energy even at 10 T.

In high magnetic fields and at low temperatures, when the Fermi level is sharp, (Fig. 7), we can adjust the bias to have the following two conditions for a given impurity. At lower bias, only the lower energy spin state channel is active for conduction, and the current is given by

$$I_1 = pe\Gamma_{cl}. \tag{2}$$

At higher bias, the higher energy spin state channel is also active for conduction, and the current is given by

$$I_2 = p'e\Gamma_{cl} = (2p - p^2)e\Gamma_{cl}, \tag{3}$$

where $p' = (2p - p^2)$ is the probability of occupying either the lower or the higher state, but not both of them. Both states cannot be occupied at the same time due to the large Coulomb energy required for another electron to simultaneously occupy the second state. For this system the single electron Coulomb charging energy ($U_C = e^2/2C$ where C is the effective capacitance of the double barrier device†) is much larger than

† $C = (\epsilon_0 k\pi r_0^2)(d_t^{-1} + d_b^{-1})$, where k is the dielectric constant, d_t and d_b are the top and bottom barrier thicknesses and r_0 is the radius of the lateral region affected by the localized impurity state in the quantum well. We take r_0 as the Bohr radius of hydrogenic impurities in GaAs (≈ 100 Å) and obtain $U_C \approx 9$ meV. Although taking r_0 as the Bohr radius is only an approximation, we obtain $U_C \geq \Delta E$ even for r_0 seven times larger.

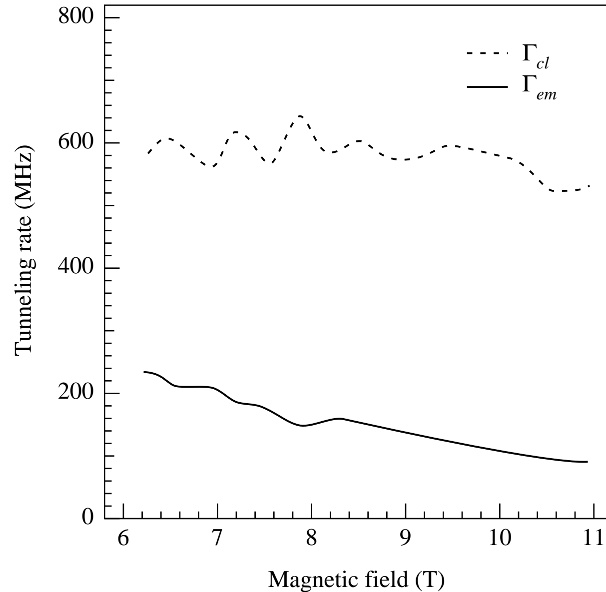

Fig. 8. Tunneling rates Γ_{em} and Γ_{cl} as a function of the magnetic field strength perpendicular to current for the 8.5 nm barrier device in forward bias orientation.

the spin splitting energy ΔE. Here we have assumed that the tunneling rates are the same at the two different biases which is a good assumption since the bias difference is much smaller than the barrier potential.

In the extreme limits these equations indicate that for $\Gamma_{cl} \gg \Gamma_{em}$, $p \approx 0$ and $I_2 \approx 2I_1$ while for $\Gamma_{cl} \ll \Gamma_{em}$, $p \approx 1$ and $I_2 \approx I_1$. This qualitatively explains the behaviour observed in Fig. 3. To get a quantitative understanding, we solve equations (2) and (3), using I_1 and I_2, to determine p. For the first impurity at 9 T, $p = 0.21$ for forward bias and $p = 0.62$ for reverse bias. A high p value indicates that the electron tunneling rate through the collector (downstream) barrier (Γ_{cl}) is lower than that through the emitter (upstream) barrier (Γ_{em}) causing an accumulation in the well. A higher p value for reverse bias (as compared to forward bias) suggests an asymmetry in the heterostructure growth with one barrier being slightly thicker than the other barrier. In forward bias the top barrier is the emitter barrier while in reverse bias the top barrier is the collector barrier. This implies that the top barrier is slightly thicker than the bottom barrier. This is consistent with the difference in the measured α values, observed asymmetry in the $I(V)$ characteristics for this sample (the main resonance peak voltage and peak current values are higher for reverse bias as compared to forward bias), and is in agreement with previous characterization [16].

We also obtain the absolute magnitude of the electron tunneling rates through the two potential barriers and study their dependence upon the magnetic field perpendicular to the current direction. Figures 8 and 9 show the tunneling rates in forward bias and reverse bias orientations respectively. Note that Γ_{em} is smaller than Γ_{cl} in forward bias orientation while Γ_{cl} is smaller than Γ_{em} in reverse bias orientation. This is because p is smaller than 0.5 in forward bias while it is larger than 0.5 in reverse bias. As mentioned before this asymmetry suggests that the top barrier of the heterostructure is slightly thicker than the bottom barrier.

Despite the asymmetry, we observe that in either orientation Γ_{em} decreases with field strength while Γ_{cl} is approximately constant. Γ_{em} roughly decreases by a factor of two as the field increases from 6 to 11 T in both bias orientations. (The oscillations in the tunneling rate are probably due to the fine structure observed on the current plateaus and its movement in magnetic field [9] not reported in this paper.) The suppression of Γ_{em}

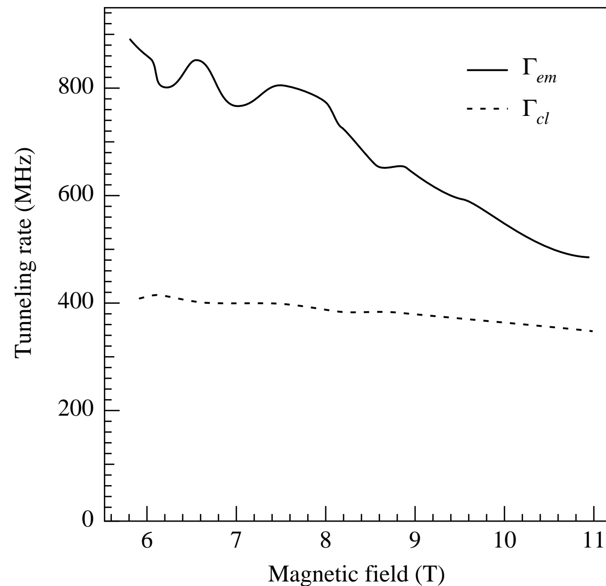

Fig. 9. Tunneling rates Γ_{em} and Γ_{cl} as a function of the magnetic field strength perpendicular to current for the 8.5 nm barrier device in reverse bias orientation.

results in the observed plateau current suppression with magnetic field [17]. This indicates that the magnetic field affects the emitter-to-well tunneling process (Γ_{em}) more than it affects the well-to-collector tunneling process (Γ_{cl}). We therefore expect more current suppression when the current is emitter barrier limited than when it is collector barrier limited, which is observed (Fig. 3). For forward bias (thicker emitter) the current at 9 T is suppressed by a factor of 41% (as compared to 0 T), while the suppression is only 20% for reverse bias (thicker collector).

We have presented a $g^*_\perp$ measurement for a given epitaxial structure. This method can be used for a precise determination of g^* as a function of quantum well width and magnetic field orientation to compare to theory. This technique generalizes to other measurements of interest such as $g^*(B)$ dependence, the investigation of magnetic impurities, different heterojunction material systems, and the determination of tunneling rates for bandgap engineered structures of interest.

Acknowledgements—We thank Prof. D. E. Prober and Dr. M. Amman for many useful discussions, C. L. Fernando and Prof. W. R. Frensley for help with the modelling, and A. Mittal for experimental assistance. This work is supported by NSF DMR-9112497 and 9216121.

References

[1] M. A Reed *et al*. Phys. Rev. Lett. **60**, 535 (1988).
[2] S. Tarucha, Y. Hirayama, T. Saku and T. Kimura, Phys. Rev. **B 41**, 5459 (1990).
[3] M. Teowordt *et al*. Phys. Rev. **B 46** 3948 (1992).
[4] B. Su, V. J. Goldman and J. E. Cunningham, Phys. Rev. **B 46**, 7644 (1992).
[5] J. W. Sleight *et al*. Phys. Rev. **B 53**, 15727 (1996).
[6] M. W. Dellow *et al*. Phys. Rev. Lett. **68**, 1754 (1992); J. W. Sakai *et al*. Appl. Phys. Lett. **64**, 2563 (1994).
[7] M. R. Deshpande *et al*. Proceedings of the IEEE/Cornell Conference on Advanced Concepts in High Speed Semiconductor Devices and Circuits, p. 177 (1993).

[8] A. K. Geim *et al*. Phys. Rev. Lett. **72**, 2061 (1994).
[9] M. R. Deshpande *et al*. in *22 International Conference on the Physics of Semiconductors*, Edited by D. J. Lockwood, Singapore: World Scientific p 1899 (1995).
[10] J. W. Sakai *et al*. Solid-State Electronics **37**, 965 (1994).
[11] M. R. Deshpande *et al*. Phys. Rev. Lett. **76**, 1328 (1996).
[12] E. L. Ivchenko and A. A. Kiselev, Sov. Phys. Semicond. **26**, 827 (1992).
[13] M. J. Snelling *et al*. Phys. Rev. **B 44**, 11345 (1991); M. J. Snelling *et al*. Phys. Rev. **B 45**, 3922 (1992).
[14] R. M. Hannak *et al*. Solid State Commun. **93**, 313 (1995).
[15] We assume sequential tunneling because the barriers are thick (85 Å). S. Luryi, Appl. Phys. Lett. **47**, 490 (1985).
[16] M. A. Reed *et al*. Appl. Phys. Lett. **54**, 1256 (1989).
[17] J. W. Sakai *et al*. Phys. Rev. **B 48**, 5664 (1993).